

Cite this: *Dalton Trans.*, 2018, **47**,  
9804Alkyltin clusters: the less symmetric Keggin  
isomers†Danielle C. Hutchison,<sup>a</sup> Rebecca D. Stern,<sup>b</sup> Morgan R. Olsen,<sup>a</sup> Lev N. Zakharov,<sup>a</sup>  
Kristin A. Persson<sup>b,c</sup> and May Nyman<sup>b,\*</sup>

The Keggin structure is prevalent in nature and synthesis, self-assembled from many metals across the periodic table as both isolated clusters and building blocks of condensed framework oxides. Here we present a one-step synthesis to obtain the sodium-centered butyltin Keggin ion in high yield and high purity, important for mechanistic nanolithography studies. Extensive solution characterization (small-angle X-ray scattering, <sup>1</sup>H, <sup>13</sup>C and <sup>119</sup>Sn nuclear magnetic resonance, electrospray mass spectrometry) also confirms solutions contain only the Na-centered dodecamers. We report three butyltin Keggin structures: the β-isomer (β-NaSn<sub>12</sub>), the γ-isomer (γ-NaSn<sub>12</sub>), and a γ-isomer capped with an additional butyltin (γ-NaSn<sub>13</sub>). All Keggin ions presented here have the general formula [NaO<sub>4</sub>BuSn<sub>12</sub>(OCH<sub>3</sub>)<sub>12</sub>(O,OH)<sub>12</sub>] (Bu = butyl), and are of neutral charge. The lack of counterions (OH<sup>-</sup>) facilitates mechanistic lithographic studies without inference from hydrolysis chemistry. The methanol reaction media enables solubility and ligates the cluster, both important to obtain high purity materials. Despite the monospecific nature of the NaSn<sub>12</sub> solutions, NMR reveals both isomer interconversion and ligand exchange. DFT computational comparisons of our three isolated structures, the capped β-isomer (β-NaSn<sub>13</sub>), along with hypothetical α-isomers (α-NaSn<sub>12</sub> and α-NaSn<sub>13</sub>), showed that the stability ranks β-NaSn<sub>12</sub> > γ-NaSn<sub>12</sub> > α-NaSn<sub>12</sub>, consistent with experimental observation. The uncapped isomers were computationally determined to be more stable than the respective capped analogues. These clusters provide a unique opportunity to investigate the lower-symmetry Keggin isomers, and to determine structural factors that control isomer selectivity as well as isomer labilization.

Received 15th May 2018,

Accepted 1st July 2018

DOI: 10.1039/c8dt01950a

rsc.li/dalton

## Introduction

The Keggin cluster, first structurally characterized in 1934, is important in metal-oxyhydroxide chemistry in both nature and synthetic inorganic chemistry.<sup>1–5</sup> The Keggin structure consists of four trimers of edge-sharing octahedra, bridged by oxo, hydroxyl, or other coordinating ligands, surrounding a central tetrahedral oxoanion. The five rotational isomers of the Keggin structure are denoted by the Greek letters α, β, γ, δ, and ε, and differ in their symmetry and the nature of connectivity between the trimers (edge-sharing vs. corner-sharing).<sup>6</sup> The α and β isomers feature all corner-sharing between the trimers

and are respectively *T<sub>d</sub>* and *C<sub>3v</sub>* symmetry. The γ-isomer has one edge-linkage and five corner-linkages between the trimers, with *C<sub>2v</sub>* symmetry. The δ-isomer is also of *C<sub>3v</sub>* symmetry, but with three corner linkages and three edge linkages. Finally, the ε-isomer features all edge-sharing between the trimers, also with *T<sub>d</sub>* symmetry.

The group V/VI (Nb, Mo and W) polyoxometalates (POMs) have the most extensive structural variations of the Keggin cluster, with both lacunary fragments and larger aggregates of these fragments. The α, and to a lesser extent, the β geometries dominate POM chemistry. Additionally, group 13 polycations (mainly Al and Ga) crystallize predominantly as δ and ε isomers, and derivatives thereof.<sup>7–13</sup> Meanwhile, Keggin structures have been isolated from across the periodic table featuring open shell transition metals, with and without organic ligands.<sup>14–16</sup> While the more symmetric isomers; particularly cubic α and ε, are favored by different metals, the tin Keggin ions uniquely favor the less symmetric β and γ isomers. This provides a new perspective for understanding this fundamental structure type, and the chemistries that adopt this structure type.

Two sodium-centered Sn Keggin structures have been isolated previously – we reported the β-butyltin Keggin ion

<sup>a</sup>Department of Chemistry, Oregon State University, 153 Gilbert Hall, Corvallis, Oregon 97331, USA. E-mail: may.nyman@oregonstate.edu

<sup>b</sup>Department of Materials Science and Engineering, University of California Berkeley, Berkeley, California 94720, USA

<sup>c</sup>Lawrence Berkeley National Laboratory, Berkeley, CA 94720, USA

† Electronic supplementary information (ESI) available: BVS calculations for oxygens of β-NaSn<sub>12</sub>, γ-NaSn<sub>12</sub>, and γ-NaSn<sub>13</sub>; complete ESI-MS peak assignments and simulations; size distribution and modelling of SAXS data; FTIR spectrum of β,γ-NaSn<sub>12</sub>. CCDC 1838234–1838236. For ESI and crystallographic data in CIF or other electronic format see DOI: 10.1039/c8dt01950a

( $\beta$ -NaSn<sub>13</sub>) in 2017, and Reuter reported the  $\gamma$ -Keggin in 1991.<sup>17,18</sup> Most chemically similar to the organotin clusters, organoantimony  $\delta$  and  $\epsilon$  Keggin ions were also reported.<sup>19</sup> Another dodecameric organotin cluster (termed the football cluster) has been known in the literature for nearly 30 years.<sup>20–22</sup> The football cluster  $\{(\text{RSn})_{12}\text{O}_{14}(\text{OH})_6\}^{12+}$ ; denoted Sn<sub>12</sub>, is composed of a hexameric ring of 5-coordinate tin, capped on each side of the ring by two trimers of octahedral tin. The overall cluster has a charge of +2 and each tin has one organic terminal ligand (isopropyl, butyl, phenyl, *etc.*). Recently, the football cluster has shown promise as a precursor for nanolithography of films deposited from these clusters.<sup>23</sup> The tin Keggin ions are likewise of potential importance for this application; in particular for benchmarking understanding of lithographic mechanisms. Our previously-isolated  $\beta$ -NaSn<sub>13</sub> was recrystallized from commercial BuSnOOH, required two recrystallization steps to obtain a pure product, and yielded inconsistent results, due to inhomogeneity in the BuSnOOH crude material.<sup>17,24</sup> The poor reproducibility and low yields hampers further applications studies. Therefore, moving forward, we have now developed a one-step, high yield, 24 h synthesis that produces a crystalline mixture of  $\beta$ -NaSn<sub>12</sub> and  $\gamma$ -NaSn<sub>12</sub>.

Here we report single-crystal X-ray structures of an uncapped  $\beta$ -Keggin ion ( $\beta$ -NaSn<sub>12</sub>), an uncapped  $\gamma$ -Keggin ion ( $\gamma$ -NaSn<sub>12</sub>), and a capped  $\gamma$ -Keggin ion ( $\gamma$ -NaSn<sub>13</sub>), as well as extensive solution characterization of the  $\beta$ , $\gamma$ -NaSn<sub>12</sub> mixture. The only way to determine the Keggin isomers is by single-crystal X-ray diffraction. Electrospray ionization mass spectrometry (ESI MS) is blind to the different isomers, but reveals the presence of compositionally pure phase NaSn<sub>12</sub>, while small-angle X-ray scattering (SAXS) shows a monospecific solution, without inference of either larger or smaller aggregates. Nuclear magnetic resonance studies (NMR; <sup>1</sup>H, <sup>13</sup>C, <sup>119</sup>Sn) show complex spectra with broadened, poorly resolved peaks. This is the only solution phase indication that the clusters are not only of mixed isomer forms, but also isomerize and undergo ligand exchange in solution.

We have also employed density functional theory (DFT) computations to help us better understand the relative stabilities of different Sn Keggin structures, particularly considering the apparent ease of  $\beta$ - $\gamma$  isomerization. We have compared our four experimentally isolated structures ( $\beta$ -NaSn<sub>12</sub>,  $\beta$ -NaSn<sub>13</sub>,  $\gamma$ -NaSn<sub>12</sub>, and  $\gamma$ -NaSn<sub>13</sub>) as well as two theoretical  $\alpha$ -Keggin ions ( $\alpha$ -NaSn<sub>12</sub> and  $\alpha$ -NaSn<sub>13</sub>). The few studies that computationally model organotin compounds focused primarily on monomeric species.<sup>25–28</sup> Prior theoretical and experimental investigations on Keggin ion stability have focused mainly on polyoxometalates<sup>29–35</sup> or aluminum polycations,<sup>14,36–38</sup> with the exception of one computational study comparing the five rotational isomers of an organoantimonate Keggin.<sup>39</sup> Here we show a stability order of  $\beta$ -NaSn<sub>12</sub> >  $\gamma$ -NaSn<sub>12</sub> >  $\alpha$ -NaSn<sub>12</sub>, and the capped clusters are all less stable, showing the same order. This is both consistent with experimental observation of these structures, and contrasts Keggin isomer stability of other chemistries. We offer some insight as to why these clusters of

lower symmetry are more stable than the higher symmetry isomers.

## Experimental

All reagents and solvents were purchased from commercial suppliers and used without further purification.

### Synthetic procedure 1

Stock solutions of 0.1 M *n*-BuSnCl<sub>3</sub> (97%) in methanol and 0.1 M NaOH in methanol were combined in a 1 : 4 Sn : OH ratio at room temperature, resulting in a total solution volume of 10 mL (2 mL of BuSnCl<sub>3</sub> and 8 mL of NaOH). Colorless needle-like crystals began to form in the closed vial in 2–4 hours and crystallization was complete within 24 hours. Single crystal and powder X-ray diffraction revealed these crystals to be a mixture of  $\beta$ -NaSn<sub>12</sub> and  $\gamma$ -NaSn<sub>12</sub>, both having the same formula and charge: [(BuSn)<sub>12</sub>(NaO<sub>4</sub>)(OCH<sub>3</sub>)<sub>12</sub>(O)<sub>5</sub>(OH)<sub>7</sub>]. Crystals of the two different isomers are indistinguishable by eye. The yield is ~30 mg (65% based on tin).

### Synthetic procedure 2

Crystals of both  $\beta$ -[(BuSn)<sub>12</sub>(NaO<sub>4</sub>)(OCH<sub>3</sub>)<sub>12</sub>(O)<sub>5</sub>(OH)<sub>7</sub>] ( $\beta$ -NaSn<sub>12</sub>) and  $\gamma$ -[(BuSn)<sub>12</sub>(NaO<sub>4</sub>)(OCH<sub>3</sub>)<sub>11</sub>(O)<sub>7</sub>(OH)<sub>6</sub>(BuSnOCH<sub>3</sub>)] ( $\gamma$ -NaSn<sub>13</sub>) were isolated from the same closed vial of *n*-BuSnCl<sub>3</sub> (96%, 0.11 mmol) and NaOH (0.36 mmol) in 9.2 mL of methanol at room temperature.  $\beta$ -NaSn<sub>12</sub> crystallized as colorless “leaf-shaped” crystals and  $\gamma$ -NaSn<sub>13</sub> crystallized as colorless needles. Unfortunately we were unable to reproduce the crystals of  $\gamma$ -NaSn<sub>13</sub>. However this structure provides a model for computational studies and adds to the knowledge of isomers favored by alkyltin Keggin ions.

### Characterization techniques

**Small angle X-ray scattering (SAXS).** X-ray scattering data were collected on an Anton Paar SAXSess instrument using Cu-K $\alpha$  radiation (1.54 Å) and line collimation. The instrument was equipped with a 2-D image plate for data collection in the  $q = 0.018$ – $2.5 \text{ \AA}^{-1}$  range. The lower  $q$  resolution is limited by the beam attenuator. Approximately 20 mmolar solutions were measured in 1.5 mm glass capillaries (Hampton Research). Scattering data of neat solvent was collected for background subtraction. Scattering was measured for 30 min for every experiment. We used SAXSQUANT software for data collection and treatment (normalization, primary beam removal, background subtraction, desmearing, and smoothing to remove the extra noise created by the desmearing routine). All analyses and curve-fitting to determine  $R_g$ , size, shape and size distribution were carried out utilizing IRENA macros with IgorPro 6.3 (Wavemetrics) software.<sup>40</sup> To simulate scattering data from the crystal structure, we used SolX software.<sup>41</sup>

**Nuclear magnetic resonance spectroscopy (NMR).** <sup>1</sup>H, <sup>13</sup>C, and <sup>119</sup>Sn NMR spectra were collected on a Bruker Ascend spectrometer (500 MHz for <sup>1</sup>H, 125 MHz for <sup>13</sup>C, 186 MHz for <sup>119</sup>Sn) with a 5 mm BBO probe at 25.0 °C. Chemical shifts are

reported in parts per million ( $\delta$ ) and  $^1\text{H}$  and  $^{13}\text{C}$  spectra are referenced to  $\text{C}_6\text{D}_6$  solvent signals.<sup>42</sup>  $^{119}\text{Sn}$  NMR is referenced to  $\text{SnCl}_4$  in  $\text{C}_6\text{D}_6$ .

**Electrospray ionization mass spectrometry (ESI-MS).** ESI-MS was carried out using an Agilent 6230 ESI-MS system comprised of a Time-of-Flight (TOF) mass spectrometer coupled to an electrospray ionizer. The crystallized Keggin product,  $\beta,\gamma\text{-NaSn}_{12}$ , ( $[\text{Sn}] = 1.2 \text{ mM}$ ), was dissolved in methanol and infused into the ESI-MS system at a flow rate of  $0.4 \text{ mL min}^{-1}$  using a syringe pump. The solutions were nebulized with the aid of heated  $\text{N}_2$  ( $325 \text{ }^\circ\text{C}$ ) flowing at  $8 \text{ L min}^{-1}$  and a pressure of 35 psig (241 kPa). The voltages of the capillary, skimmer, and RT octopole were set at 3500, 65, and 750 V respectively, while the voltage of the fragmenter was set at 100 V. The data were collected in the positive ionization mode. No ion species were detected in the negative ionization mode.

**Single-crystal X-ray diffraction data collection analysis.** Diffraction intensities for  $\beta\text{-NaSn}_{12}$  (CCDC 1838234 $\dagger$ ),  $\gamma\text{-NaSn}_{13}$  (CCDC 1838235 $\dagger$ ), and  $\gamma\text{-NaSn}_{12}$  (CCDC 1838236 $\dagger$ ), were collected at 153 K ( $\beta\text{-NaSn}_{12}$ ), 150 K ( $\gamma\text{-NaSn}_{13}$ ) and 173 K ( $\gamma\text{-NaSn}_{12}$ ) on a Bruker Apex2 DUO CCD diffractometer using  $\text{CuK}\alpha$  radiation,  $\lambda = 1.54178 \text{ \AA}$ . Absorption corrections were applied by SADABS.<sup>43</sup> Space groups were determined based on systematic absences. Structures were solved by direct methods and Fourier techniques and refined on  $F^2$  using full matrix least-squares procedures. All non-H atoms were refined with anisotropic thermal parameters except C atoms in the disordered terminal butyl groups which were refined with isotropic thermal parameters. All H atoms were refined in calculated positions in a rigid group model. Diffraction for all three samples is very weak at high angles. Even using a strong Incoatec  $\mu\text{S}$  Cu source for  $\beta\text{-NaSn}_{12}$  and  $\gamma\text{-NaSn}_{13}$  it was possible to collect diffraction data only up  $2\theta_{\text{max}} = 107.9$  and  $108.78^\circ$ , respectively. Statistics of the reflections at the high angles are poor and it reduce structure resolution. However, it provides an appropriate number of reflections per number of refined parameters; 5787/542 ( $\beta\text{-NaSn}_{12}$ ) and 12160/952 ( $\gamma\text{-NaSn}_{13}$ ). Terminal  $n\text{-Bu}$  groups in all structures are highly disordered; there are strong elongations for many C atoms and some groups were treated as being disordered over two positions. Terminal  $n\text{-Bu}$  groups in all structures were refined with restrictions; the standard bond distances have been used in the refinements as the targets for corresponding bonds. All structures were refined applying a rigid bond restrains; RIGU option in SHELX package. It should be mentioned that on the residual density for  $\gamma\text{-NaSn}_{12}$  there are two relatively high peaks (4.77 and 4.67  $\text{e \AA}^{-3}$ ) located above three  $\mu_2$ -bridging O atoms, but not consistent with any atoms based on chemical information. We considered  $\beta/\gamma$  isomer disorder in the lattice as an explanation. We overlay the two isomers (including the  $q$ -peaks for  $\gamma$ ) to determine if these peaks aligned with any atoms of the  $\beta$ -isomer, and found this is not the case. All calculations were performed by the Bruker SHELXL-2014/7 package.<sup>44</sup>

**Powder X-ray diffraction analysis.** Powder X-ray diffraction data was performed on Rigaku Ultima-IV at  $25 \text{ }^\circ\text{C}$  with  $\text{Cu K}\alpha$

radiation. The diffraction patterns were obtained in the range from  $3$  to  $60^\circ$  ( $2\theta$ ) with a scan speed of  $2^\circ \text{ min}^{-1}$  and step size of  $0.03^\circ$ .

**Fourier transform infrared spectroscopy.** (FTIR) spectra were recorded on a Nicolet iS10 FTIR spectrometer with a secondary Nicolet iZ 10 module purchased from Thermo Fisher Scientific Inc. The instrument was equipped with a diamond plate for attenuated total reflectance (ATR) measurements. Spectra were collected in air from crushed crystals of  $\beta,\gamma\text{-NaSn}_{12}$ . This spectrum can be found in the ESI. $\dagger$

### Computational methods

The computational results were obtained using Gaussian 09 (full authorship in ESI $\dagger$ ).<sup>45</sup> The geometry of each cluster was first optimized in the gas phase using the B3LYPfunctional.<sup>46</sup> The basis set 6-31G(d) was used for elements Na, C, H, and O, while the basis set LANL2DZ was used for the element Sn.<sup>47,48</sup> Subsequently, with the same level of theory, a frequency calculation was done to verify the absence of imaginary vibration modes to confirm that the system was in a stable/metastable state. An effective core potential LANL2DZ was used for Sn. The geometry was further optimized in water using the continuum solvation model SMD.<sup>49</sup> The electronic energy was refined using the B3LYP single point with the basis set 6-311+G(d,p) for elements Na, C, H, and O, and basis set LANL2DZ for Sn.<sup>50</sup> The solvation energy was found using B3LYP/6-31G(d) single point with SMD for water.

## Results and discussion

### Synthesis discussion

The synthesis of  $\text{Sn}_{12}$  with hydroxide counterions reported by Eychenne-Baron and Sanchez is lengthy and complex, involving various purification and ion exchange steps.<sup>21</sup> Therefore it is difficult to reproduce, has low yields, and often contains impurities due to incomplete ion exchange. While  $\text{Sn}_{12}$  is important to provide a Na-free molecule for microelectronic applications, the  $\text{NaSn}_{12}$  clusters provide nearly identical chemistry for film deposition and patterning. Thereby, with its simple and reproducible chemical synthesis reported here, it can serve as a readily-obtained proxy for studying lithographic mechanisms. The synthetic procedure for  $\text{NaSn}_{12}$  involves just one step, at room temperature, and it can be performed in a 20 ml vial. Stock solutions of 0.1 M  $\text{BuSnCl}_3$  in methanol and 0.1 M  $\text{NaOH}$  in methanol are combined in a 1 : 4 ratio (usually 2 mL of  $\text{BuSnCl}_3$  to 8 mL of  $\text{NaOH}$ ) at room temperature and crystallization is complete within 24 hours. This synthetic procedure is highly reproducible and does not require any heating, filtration, or recrystallization. Although our reaction produces a mixture of  $\beta\text{-NaSn}_{12}$  and  $\gamma\text{-NaSn}_{12}$ , both clusters have the same formula and 0-valency, and no counterions or other impurities appear to be present (discussed later). While hydroxides are ideal counterions for film deposition in that they are eliminated by mild heating, their presence can result in undesirable background hydrolysis that compromises sharp

turn-on of solubility contrast by radiation-promoted linking of clusters.

### Description of structures

The pertinent data for the three reported structures is summarized in Table 1. The clusters  $\beta$ -NaSn<sub>12</sub>,  $\gamma$ -NaSn<sub>12</sub>, and  $\gamma$ -NaSn<sub>13</sub> all possess the Keggin framework (Fig. 1). In these clusters, each trimer consists of three edge-sharing BuSnO<sub>5</sub> octahedra with the butyl group serving as the terminal ligand

on all tin atoms. The central atom in all three Keggin structures is Na. The twelve bridging oxygens within the trimers (three O<sup>2-</sup> in each of the four trimers) are methoxy ligands and the bridging oxygens between the four trimers are oxo or hydroxyl ligands. The BuSn cap of  $\gamma$ -NaSn<sub>13</sub> is 5-coordinate with 3 bonds to the cluster and two terminal ligands (butyl and methoxy). It is located in one of the pentagonal windows that are positioned on either side of the two edge-sharing trimers (Fig. 1). One exception to the locations of the methoxy

**Table 1** Crystallographic information for reported structures

Compound	$\beta$ -NaSn <sub>12</sub>	$\gamma$ -NaSn <sub>12</sub>	$\gamma$ -NaSn <sub>13</sub>
Moiety formula	[(BuSn) <sub>12</sub> (NaO <sub>4</sub> )(OCH <sub>3</sub> ) <sub>12</sub> (O) <sub>5</sub> (OH) <sub>7</sub> ]	[(BuSn) <sub>12</sub> (NaO <sub>4</sub> )(OCH <sub>3</sub> ) <sub>12</sub> (O) <sub>5</sub> (OH) <sub>7</sub> ]	[(BuSn) <sub>12</sub> (NaO <sub>4</sub> )(OCH <sub>3</sub> ) <sub>11</sub> (O) <sub>7</sub> (OH) <sub>6</sub> (BuSnOCH <sub>3</sub> )]
Empirical formula	C <sub>60</sub> H <sub>151</sub> NaO <sub>28</sub> Sn <sub>12</sub>	C <sub>60</sub> H <sub>151</sub> NaO <sub>28</sub> Sn <sub>12</sub>	C <sub>64</sub> H <sub>159</sub> NaO <sub>29</sub> Sn <sub>13</sub>
Molecular weight [g mol <sup>-1</sup> ]	2768.07	2768.07	2958.86
<i>T</i> [K]	153 ± 2	173 ± 2	150 ± 2
Crystal system	Orthorhombic	Monoclinic	Monoclinic
Space group	<i>Pbcm</i>	<i>P2<sub>1</sub>/c</i>	<i>P2<sub>1</sub>/n</i>
<i>a</i> [Å]	16.1584(6)	19.0758(6)	24.0683(8)
<i>b</i> [Å]	24.8434(11)	24.1794(10)	18.8014(6)
<i>c</i> [Å]	23.5910(10)	21.0889(7)	24.5975(7)
$\alpha$ [°]	90	90	90
$\beta$ [°]	90	94.047(2)	113.8910(17)
$\gamma$ [°]	90	90	90
Volume [Å <sup>3</sup> ]	9470.1(7)	9702.8(6)	10 177.1(6)
<i>Z</i>	4	4	4
$\rho_{\text{calcd}}$ [Mg cm <sup>-3</sup> ]	1.941	1.895	1.931
$\mu$ [mm <sup>-1</sup> ]	25.273	24.667	25.454
<i>F</i> (000)	5384	5384	5744
Crystal size [mm]	0.150 × 0.080 × 0.040	0.120 × 0.090 × 0.080	0.140 × 0.120 × 0.090
Radiation [Å]	1.54178	1.54178	1.54178
2 $\theta$ range for data collection [°]	2.735 to 53.947	2.322 to 66.724	2.167 to 54.039
Index ranges	-14 ≤ <i>h</i> ≤ 16 -25 ≤ <i>k</i> ≤ 23 -24 ≤ <i>l</i> ≤ 20	-22 ≤ <i>h</i> ≤ 19 -20 ≤ <i>k</i> ≤ 28 -25 ≤ <i>l</i> ≤ 21	-24 ≤ <i>h</i> ≤ 25 -18 ≤ <i>k</i> ≤ 19 -25 ≤ <i>l</i> ≤ 25
Reflections collected	34 416	53 009	74 384
Independent reflections/ <i>R</i> <sub>int</sub>	5787 [ <i>R</i> (int) = 0.0680]	17 123 [ <i>R</i> (int) = 0.0749]	12 160 [ <i>R</i> (int) = 0.0859]
Data/restraints/parameters	5787/803/542	17 123/1520/909	12 160/1548/952
Goodness of fit on <i>F</i> <sup>2</sup>	1.056	1.051	1.059
<i>R</i> <sub>1</sub> / <i>wR</i> <sub>2</sub> [ <i>I</i> > 2 $\sigma$ ( <i>I</i> )]	0.0720/0.1765	0.0750/0.1934	0.0857/0.2133
<i>R</i> <sub>1</sub> / <i>wR</i> <sub>2</sub> [all data]	0.1143/0.2131	0.1384/0.2397	0.1315/0.2601
largest diff. peak/hole [e Å <sup>-3</sup> ]	1.359 and -0.961	4.770 and -1.057	2.033 and -1.744

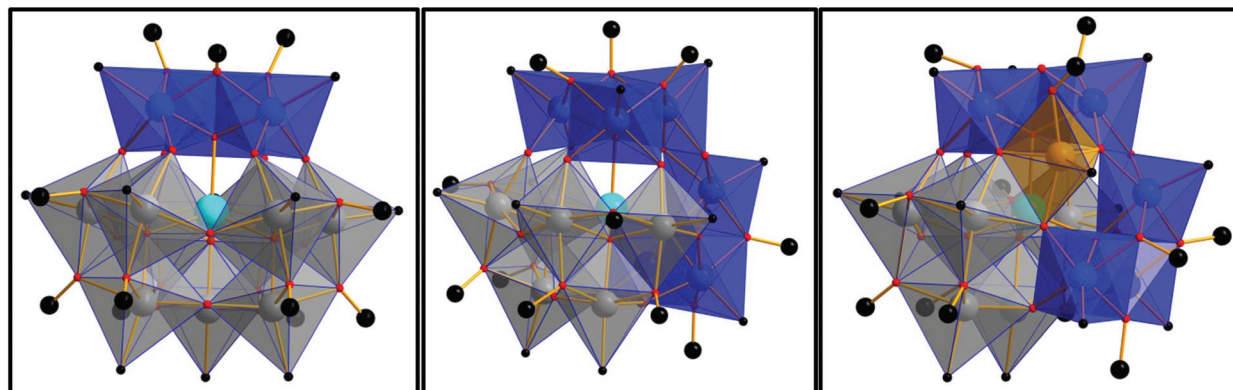


**Fig. 1** Crystal structures of  $\beta$ -NaSn<sub>12</sub> (left),  $\gamma$ -NaSn<sub>12</sub> (center), and  $\gamma$ -NaSn<sub>13</sub> (right). Tin atoms are represented by blue, gray, and orange polyhedra. Blue polyhedra represent trimers which have been rotated 60° with respect to the  $\alpha$ -configuration. The orange polyhedron on  $\gamma$ -NaSn<sub>13</sub> represents the additional capping tin. Na is shown in turquoise at the center of each cluster. Only the carbon that is bound directly to Sn is shown, for ease of viewing.

and oxo/hydroxyl ligands is found in the structure of  $\gamma$ -NaSn<sub>13</sub>. One bridging oxygen within the trimer near the capping tin is a hydroxyl ligand rather than the expected methoxy. This could be a result of steric constraints due to the proximity of the capping tin, in addition to the fact that the methoxy ligands appear to be fairly labile (discussed later).

No counterions were located in any of the three lattices, indicating that  $\beta$ -NaSn<sub>12</sub>,  $\gamma$ -NaSn<sub>12</sub>, and  $\gamma$ -NaSn<sub>13</sub> all have a neutral charge. Bond valence sum (BVS) calculations for the oxygens of  $\beta$ -NaSn<sub>12</sub>,  $\gamma$ -NaSn<sub>12</sub>, and  $\gamma$ -NaSn<sub>13</sub> can be found in the ESI (Tables SI1, SI2, and SI3† respectively), which distinguished oxos from hydroxyls (see formulae above). Several BVS values for the bridging oxygens were ambiguous, with values falling between 1.2 and 1.4. A cutoff value to distinguish oxos from hydroxyls was determined for each structure, so that each formula contained the correct number of oxos and hydroxyls to be consistent with a neutral charge. For  $\gamma$ -NaSn<sub>12</sub>, oxygens with a BVS of 1.35 or greater were assigned as O<sup>2-</sup>, and the remaining oxygens were assigned as OH<sup>-</sup>. For  $\gamma$ -NaSn<sub>13</sub>, oxygens with a BVS of 1.31 or greater were assigned as O<sup>2-</sup>. For  $\beta$ -NaSn<sub>12</sub> however, some of the protons must be disordered over symmetrically identical sites in order to have the appropriate charge. Oxygens with a BVS of 1.38 or greater were assigned as O<sup>2-</sup>, accounting for four of the five required oxo ligands. The two oxos with a BVS of 1.35 are mixed occupancy /O<sup>2-</sup>/OH<sup>-</sup>. Hydroxyl/oxo disorder and ambiguity is also common in polyoxometalate crystal structures.

### Evidence for mixed $\beta/\gamma$ isomers in bulk solid

Powder X-ray diffraction of ground crystals shows a broad peak between 5–10° 2 $\theta$ , and no other significant features (Fig. 2a), while the SEM image (Fig. 2b) shows good crystallinity. Simulated powder patterns for  $\beta$ -NaSn<sub>12</sub> and  $\gamma$ -NaSn<sub>12</sub> from the single crystal data are similar to each other and consistent with the experimental data. The apparent poor crystallinity of the ground powder is typical of cluster-containing crystals; in this case due to hydrolysis of methoxy ligands upon grinding in air. While analysis of multiple individual crystals revealed a mixture of  $\beta$ -NaSn<sub>12</sub> and  $\gamma$ -NaSn<sub>12</sub>, only one isomer was

present in each single-crystal that was assessed. This does not necessarily mean that  $\beta$ -NaSn<sub>12</sub> and  $\gamma$ -NaSn<sub>12</sub> do not crystallize in the same lattice, rather it may infer that crystals containing mixed isomers form poor quality crystals, which we were not able to analyze.

### Solution characterization

**Mass spectrometry.** The NaSn<sub>12</sub> clusters are soluble in organic media including alcohols, benzene, toluene, chloroform, THF, DMF, and 2-heptanone, so these solvents were employed for solution characterization. The ten natural isotopes of tin provide very distinctive peak envelopes of the multinuclear clusters, aiding accurate identification of the soluble species detected by mass spectrometry. The TOF ESI-MS analysis of  $\beta,\gamma$ -NaSn<sub>12</sub> crystals redissolved in methanol showed several peak envelopes, with the two most abundant peaks occurring at 2781.8808 and 2750.8555 *m/z* (Fig. 3a, positive ionization mode, 100 V fragmentation). All peak envelopes have peak separations of 1 *m/z*, indicating *a* + 1 charge. Major peak envelope assignments are shown in Fig. 3b and Table 2. The formula for  $\beta,\gamma$ -NaSn<sub>12</sub> most similar to the formula determined from X-ray structure comprises ~17% of the observed species (bold formula in Table 2). Prior mass spectral analysis of Sn<sub>12</sub> show that hydroxide ligands can be replaced by methoxy ligands in methanol solution.<sup>51</sup> The ESI-MS results likewise show extensive exchange between methoxy, oxo and hydroxyl, with multiple *m/z* formulae that differ only by the number of each ligand. The peak at 2558.6971 *m/z* contains 11 butyltin groups, likely a product of fragmentation. Additional peak simulations can be found in the ESI.†

**X-ray scattering.** Fig. 4 shows the experimental (red) and simulated (blue) scattering curves for  $\beta,\gamma$ -NaSn<sub>12</sub> in benzene.  $\beta$ -NaSn<sub>12</sub> and  $\gamma$ -NaSn<sub>12</sub> are indistinguishable by SAXS, so only the simulation for  $\gamma$ -NaSn<sub>12</sub> is shown. The experimental scattering is consistent with the simulation, indicating a pure phase solution. Size distribution and modelling of the SAXS data give a diameter of 9.1 Å and radius of 4.6 Å, respectively (Fig. SI10 and SI11†).

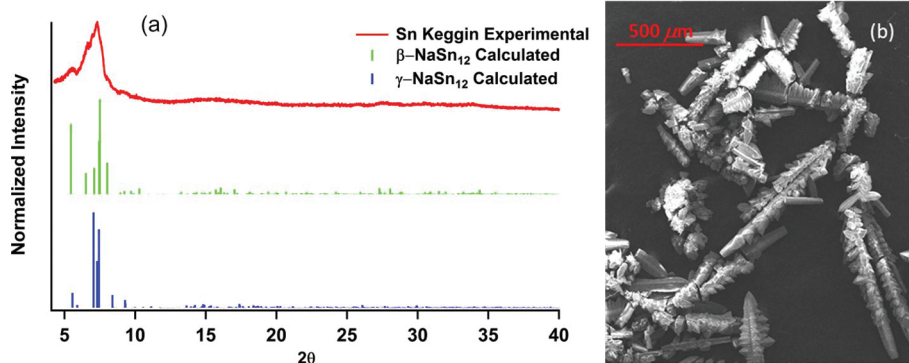


Fig. 2 (a) Experimental powder X-ray diffraction pattern for  $\beta,\gamma$ -NaSn<sub>12</sub> (red) along with calculated powder patterns for  $\beta$ -NaSn<sub>12</sub> (green) and  $\gamma$ -NaSn<sub>12</sub> (blue). (b) SEM image of  $\beta,\gamma$ -NaSn<sub>12</sub> crystals.

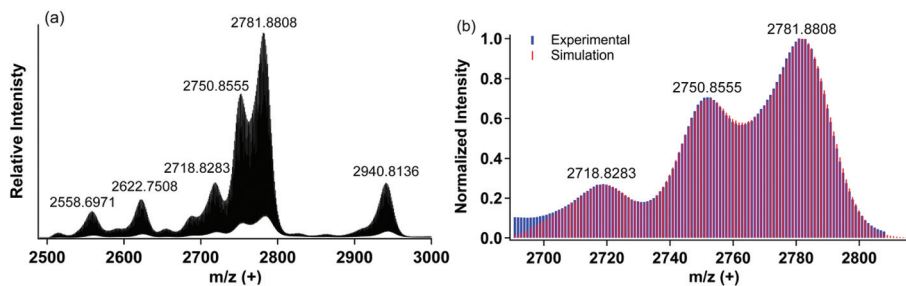


Fig. 3 (a) ESI-MS full spectrum for 0.1 mM  $\beta,\gamma$ - $\text{NaSn}_{12}$  in MeOH. Positive ionization mode, 100 V fragmentation. (b) Overlay of experimental (blue) and simulated (red) ESI-MS peak envelopes for most intense peaks of spectrum. The simulated peak envelope is a combination of 9 overlapping peaks.

Table 2 Formulae and  $m/z$  of simulated peak envelopes

Formula	$m/z$ obs.	$m/z$ calc.	% Contribution (for overlapping peaks)
$[(\text{BuSn})_{11}(\text{NaO}_4)(\text{OH})_{17}(\text{OCH}_3)_8]^{1+}$	2558.6971	2558.8656	
$[(\text{BuSn})_{12}(\text{NaO}_4)(\text{O})_{10}(\text{OH})(\text{OCH}_3)_7]^{1+}$	2590.7214	2590.7252	
$[(\text{BuSn})_{12}(\text{NaO}_4)(\text{O})_9(\text{OH})_2(\text{OCH}_3)_8]^{1+}$	2622.7508	2622.7515	
$[(\text{BuSn})_{12}(\text{NaO}_4)(\text{O})_8(\text{OH})_3(\text{OCH}_3)_9]^{1+}$	2654.7756	2654.7777	
$[(\text{BuSn})_{12}(\text{NaO}_4)(\text{O})_7(\text{OH})_4(\text{OCH}_3)_{10}]^{1+}$	2686.8016	2686.8040	
$[(\text{BuSn})_{12}(\text{NaO}_4)(\text{O})_6(\text{OH})_6(\text{OCH}_3)_{10}]^{1+}$		2704.8146	3.94%
$[(\text{BuSn})_{12}(\text{NaO}_4)(\text{O})_6(\text{OH})_5(\text{OCH}_3)_{11}]^{1+}$	2718.8283	2718.8302	8.66%
$[(\text{BuSn})_{12}(\text{NaO}_4)(\text{O})_4(\text{OH})_{11}(\text{OCH}_3)_9]^{1+}$		2726.8200	1.97%
$[(\text{BuSn})_{12}(\text{NaO}_4)(\text{O})_4(\text{OH})_{10}(\text{OCH}_3)_{10}]^{1+}$		2740.8357	5.51%
$[(\text{BuSn})_{12}(\text{NaO}_4)(\text{O})_5(\text{OH})_6(\text{OCH}_3)_{12}]^{1+}$	2750.8555	2750.8565	17.32%
$[(\text{BuSn})_{12}(\text{NaO}_4)(\text{O})_4(\text{OH})_9(\text{OCH}_3)_{11}]^{1+}$		2754.8514	7.87%
<b><math>[(\text{BuSn})_{12}(\text{NaO}_4)(\text{O})_4(\text{OH})_8(\text{OCH}_3)_{12}]^{1+}</math></b>		2768.8671	16.93%
$[(\text{BuSn})_{12}(\text{NaO}_4)(\text{O})_4(\text{OH})_7(\text{OCH}_3)_{13}]^{1+}$	2781.8808	2782.8828	34.65%
$[(\text{BuSn})_{12}(\text{NaO}_4)(\text{O})_5(\text{OH})_3(\text{OCH}_3)_{15}]^{1+}$		2792.9036	3.15%
$[(\text{BuSn})_{12}(\text{NaO}_4)(\text{O})_5(\text{OH})_{13}(\text{OCH}_3)_9(\text{CH}_3\text{OH})_9]^{1+}$	2940.8136	2940.9830	

\*Starred formulae have fewer than 40 required ligands (resulting from fragmentation). Bold formula most similar to structural formula.

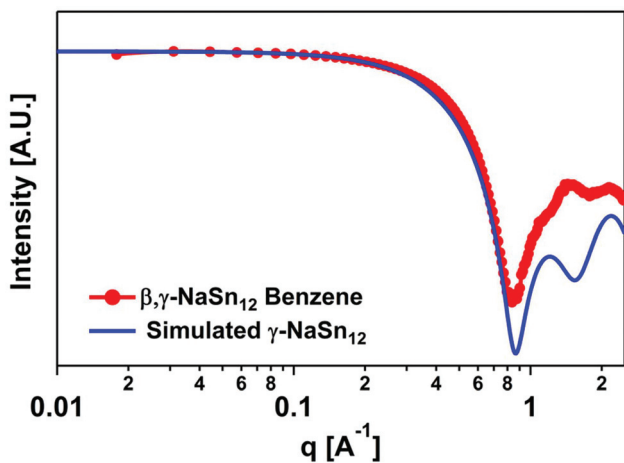


Fig. 4 Simulated (blue) and experimental (red) small angle X-ray scattering curves for  $\beta,\gamma$ - $\text{NaSn}_{12}$  in benzene. Discrepancies between the simulated and experimental curves above  $q = 0.8 \text{ \AA}^{-1}$  are due to imperfect background subtraction and solvent scattering.

**NMR.** Multinuclear ( $^1\text{H}$ ,  $^{13}\text{C}$ ,  $^{119}\text{Sn}$ ) NMR characterization of  $\beta,\gamma$ - $\text{NaSn}_{12}$ , like the ESI-MS data, suggests ligand exchange, in addition to the presence of two different isomers (Fig. 5–7).

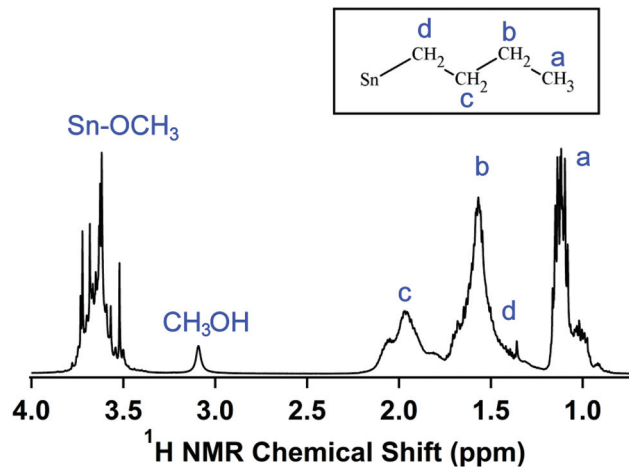


Fig. 5  $^1\text{H}$  NMR spectrum of  $\beta,\gamma$ - $\text{NaSn}_{12}$  in benzene- $d_6$ .

Peaks were assigned based on the chemical shifts of  $\beta$ - $\text{NaSn}_{13}$ .<sup>17</sup> The four chemical shifts in the  $^1\text{H}$  and  $^{13}\text{C}$  NMR spectra which correspond to the butyl chains on the cluster are broad and poorly defined, similar to the spectra for  $\beta$ - $\text{NaSn}_{13}$ . The  $^{119}\text{Sn}$  spectrum shows an overlap of peaks from  $-450$  ppm

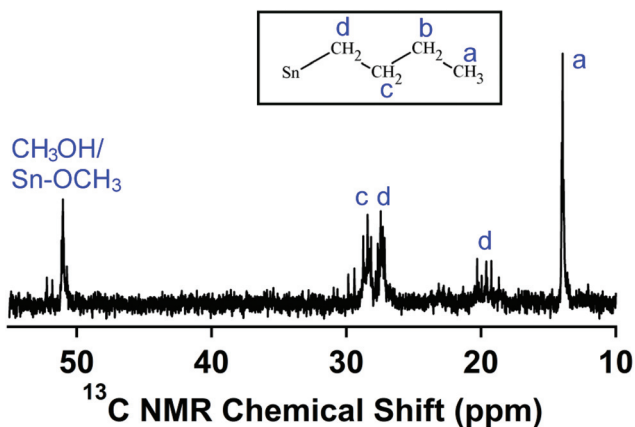


Fig. 6  $^{13}\text{C}$  NMR spectrum of  $\beta,\gamma\text{-NaSn}_{12}$  in benzene- $d_6$ .

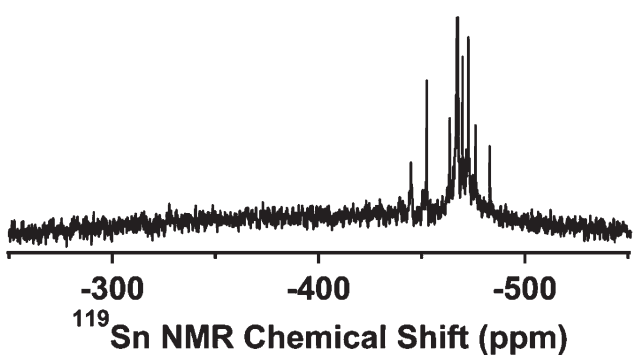


Fig. 7  $^{119}\text{Sn}$  NMR spectrum of  $\beta,\gamma\text{-NaSn}_{12}$  in benzene- $d_6$ .

to  $-500$  ppm which is consistent with a cluster (or mixture of clusters) that contains only 6-coordinate organotin species. Ideally,  $\beta\text{-NaSn}_{12}$  ( $C_{3v}$  symmetry) should have three different Sn chemical environments and  $\gamma\text{-NaSn}_{12}$  ( $C_{2v}$  symmetry) should have a total of four different Sn chemical environments. In addition to the seven symmetrically inequivalent Sn environments, there is a distribution of hydroxide/methoxy ligands amongst the clusters, shown by ESI MS. This increases the number of chemically inequivalent sites. It also appears that these effects are far-reaching. Even the protons on the butyl chain which are several bonds away from the tin are affected by ligand exchange. Similarly, prior studies suggest that changing the number or locations of protons on divacant lacunary tungstate  $\gamma\text{-Keggin}$  ions significantly changes the  $^{183}\text{W}$  NMR spectrum – increasing the number of peaks and shifting the peaks.<sup>33</sup> Those protonation states having the lowest symmetry also exhibited the largest number of chemical shifts. Future studies will focus on monitoring and quantifying ligand exchange of these clusters, and the effect of different solvents.

### Computational studies

Although there are five different rotational isomers of the Keggin ion ( $\alpha$ ,  $\beta$ ,  $\gamma$ ,  $\delta$ , and  $\epsilon$ ), we and others have only been able to experimentally isolate the  $\beta$  and  $\gamma$  isomers, both with

and without capping Sn. For those transition metals that adopt the Keggin structure (W, Mo, Nb), the  $\alpha$ -isomer is typically the most stable, closely followed by the  $\beta$ -isomer.<sup>34</sup> In contrast, the  $\text{Al}_{13}$  Keggin ion favors the  $\epsilon$  configuration which also has a high degree of symmetry; both the  $\alpha$  and the  $\epsilon$  possess  $T_d$  symmetry.<sup>7</sup> Additionally, the Al-polycations favor the  $\delta$ -isomer when capped on the unique corner-linked trimer,<sup>38</sup> and computational studies have shown the oxygens of this face are more basic, promoting binding of the capping metal cation.<sup>14</sup> Meanwhile, organoantimonate clusters favor the  $\delta$  and  $\epsilon$  isomers.<sup>19</sup> To our knowledge, no other systems exist which favor the formation of  $\beta$  and  $\gamma$  isomers. Furthermore, these two isomers have relatively low symmetry and any naturally occurring  $\beta$  or  $\gamma$  Keggin structures have yet to be identified. One might argue that higher symmetry clusters form ordered lattices more readily, which is why they are more frequently observed by this solid-state characterization method that provides absolute identification of isomers. However, this argument cannot be made for these uniquely lower-symmetry Keggin clusters. It is for these reasons that we have turned to computational modeling, to compare the relative stabilities of the  $\alpha$  (hypothetical),  $\beta$ , and  $\gamma$  tin Keggin clusters, as well as the Sn-capped analogues. For the computational comparisons, all clusters were assigned a charge of +1. Although the lack of counterions in the crystal structures indicate that all of the clusters have a neutral charge, adding one additional proton creates a more symmetrical structure (4 oxos and 8 hydroxyls for +1 charge vs. 5 oxos and 7 hydroxyls for neutral charge). The +1 charge is also consistent with the species observed by mass spectrometry. Additionally, we use methyl instead of butyl as the terminal Sn-bound ligand for computation in order to simplify the models, since disorder in the butyl chains is prevalent in single-crystal X-ray structures. The theoretical structures for  $\alpha\text{-NaSn}_{12}$  and  $\alpha\text{-NaSn}_{13}$  are shown in Fig. 8. The cap position and bonding for  $\alpha\text{-NaSn}_{13}$  were chosen to resemble the capping structure of  $\beta\text{-NaSn}_{13}$ .

The stabilities of the six Keggin structures were computationally compared using both the hydrolysis Gibbs free energy and the HOMO–LUMO gap. To reduce the number of degrees of freedom when modeling these systems and ease the com-

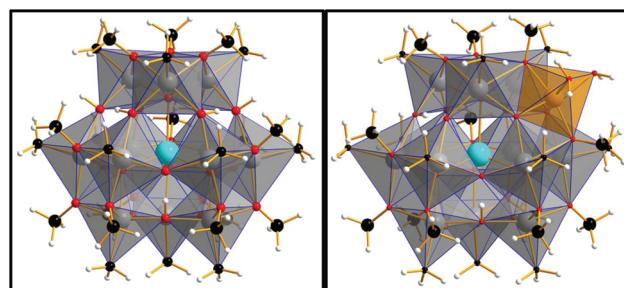


Fig. 8 Theoretical structures for  $\alpha\text{-NaSn}_{12}$  (left) and  $\alpha\text{-NaSn}_{13}$  (right). Tin atoms are represented by gray polyhedra. The orange polyhedron represents the additional capping tin on  $\alpha\text{-NaSn}_{13}$ . Na is shown as a turquoise sphere at the center of each cluster.

parison between these three structures, the uncapped  $\alpha$ ,  $\beta$ , and  $\gamma$ -isomers were all assigned the same formula and charge:  $[(\text{MeSn})_{12}(\text{NaO}_4)(\text{OCH}_3)_{12}(\text{O})_4(\text{OH})_8]^{1+}$ . The capped  $\alpha$ ,  $\beta$ , and  $\gamma$ -isomers were assigned slightly different formulae to reflect what was experimentally observed. The simulated  $\beta$ - $\text{NaSn}_{13}$  was assigned a formula of  $[(\text{MeSn})_{12}(\text{NaO}_4)(\text{OCH}_3)_{12}(\text{O})_8(\text{OH})_4(\text{Sn}(\text{H}_2\text{O})_2)]^{1+}$  which is exactly consistent with the experimental crystal structure. The experimentally characterized cap for  $\gamma$ - $\text{NaSn}_{13}$  is  $[\text{Sn}(\text{Me})(\text{OCH}_3)]^{2+}$  with 3 bonds to the cluster, and was likewise used for the computational study with a formula of  $[(\text{MeSn})_{12}(\text{NaO}_4)(\text{OCH}_3)_{12}(\text{O})_6(\text{OH})_6(\text{Sn}(\text{Me})(\text{OCH}_3))]^{1+}$ .

We used parameterized continuum solvation models to accurately determine solvation energies, using B3LYP.<sup>52</sup> We determined the hydrolysis Gibbs free energy in solution by using a thermodynamic cycle in which the hydrolysis energy is the sum of the corresponding gas-phase Gibbs free energy ( $\Delta G_{\text{gas}}$ ) and the Gibbs free energies of solvation ( $\Delta G_{\text{solv}}$ ; eqn (1)). The gas-phase Gibbs free energy contains a correction term that takes into account the enthalpy, entropy, and temperature of the system when a frequency analysis is conducted. The term “ $n$ ” is the coefficient of that species. An example of this thermodynamic cycle using  $\beta$ - $\text{NaSn}_{12}$  is shown in Scheme 1. The dielectric constant for the solvent model was set to  $\sim 78.36$ , consistent with water, and we will exploit other solvents and/or explicit solvent molecules in our future research.<sup>34,53,54</sup> The computational results are summarized in Table 3.

Hydrolysis Gibbs free energy ( $\Delta G_{\text{aq}}$ ) obtained from thermodynamic cycle in Scheme 1.

$$\Delta G_{\text{aq}} = \Delta G_{\text{gas}} + \sum_{i=1}^{N \text{ Products}} n_i \Delta G_i^{\text{solv}} - \sum_{j=1}^{N \text{ reactants}} n_j \Delta G_j^{\text{solv}} \quad (1)$$

The most stable clusters are expected to have a relatively low hydrolysis Gibbs free energy and a large HOMO–LUMO gap. The hydrolysis Gibbs free energy differences between clusters are similar in magnitude to those reported prior.<sup>34,55</sup> The stability ranking of  $\text{NaSn}_{12}$  is  $\beta$ - $\text{NaSn}_{12} > \gamma$ - $\text{NaSn}_{12} > \alpha$ - $\text{NaSn}_{12}$ ; and the uncapped clusters are more stable than their capped counterparts, under the current assumption of no explicit solvent or counterions. These results are consistent with our experimental findings.  $\beta$ - $\text{NaSn}_{12}$  appears to be the most favored, as it crystallizes under two different synthetic conditions, while  $\gamma$ - $\text{NaSn}_{12}$  and  $\gamma$ - $\text{NaSn}_{13}$  are each crystallized under different conditions and always mixed with  $\beta$ - $\text{NaSn}_{12}$ . The calculated relative instability of the  $\alpha$ -isomer is also con-

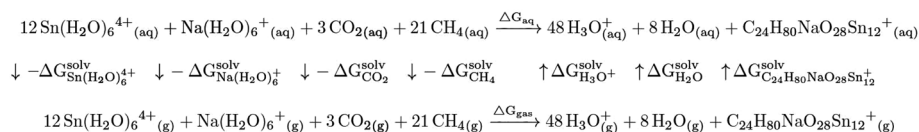
**Table 3** Hydrolysis Gibbs free energy ( $\text{kcal mol}^{-1}$ ) and HOMO–LUMO gaps of  $\text{NaSn}_{12}$  and  $\text{NaSn}_{13}$  isomers

	Hydrolysis Gibbs free energy ( $\text{kcal mol}^{-1}$ )	$\Delta G$ ( $\text{kcal mol}^{-1}$ )	Destabilization by capping ( $\text{kcal mol}^{-1}$ )	HOMO–LUMO gap (eV)
$\beta$ - $\text{NaSn}_{12}$	327.4	0	—	6.24
$\gamma$ - $\text{NaSn}_{12}$	337.4	10.0	—	5.91
$\alpha$ - $\text{NaSn}_{12}$	342.7	15.3	—	6.20
$\beta$ - $\text{NaSn}_{13}$	364.9	37.5	37.5	5.28
$\gamma$ - $\text{NaSn}_{13}$	361.2	33.8	23.8	5.80
$\alpha$ - $\text{NaSn}_{13}$	369.7	42.3	27.0	5.17

sistent with our experimental results, as it has not been ever observed experimentally.

In the  $\beta$  isomer, all of trimers are joined by corners at six points, while the  $\gamma$ -isomer has one edge-linking and five corner-linkings. The Sn–Sn edge-sharing distance is 3.26 Å, while the Sn–Sn corner-sharing distance is  $\sim 3.4$ – $3.5$  Å, causing relative instability of the  $\gamma$ -isomer from electrostatic repulsion. The lower stability of the capped clusters is contradictory to previous studies that showed capping stabilizes polyoxometalates and aluminum polycations by respectively decreasing the cluster’s overall charge or stabilizing a more negative cluster face.<sup>14,56</sup> Since all simulated clusters have the same charge in this study, the former explanation is irrelevant. Experimentally capping is charge neutral because the attachment site is converted from hydroxide to oxide. The cap on the  $\gamma$ - $\text{NaSn}_{13}$  yields a short Sn–Sn distance of 3.15 Å between the cap and the nearest tin, and destabilization may be a result of repulsion. Capping of  $\alpha$ - $\text{NaSn}_{13}$  distorts the polyhedra surrounding the capping Sn (Fig. 8), which may contribute to its destabilization. The cap on  $\beta$ - $\text{NaSn}_{13}$  does not lead to any distortion nor close Sn–Sn distances, so reasons for its destabilization are unclear.

When we consider Keggin structures from across the Periodic table, the charge of the metal cations shows a consistent trend with preferred isomers. Highly charged transition metals ( $\text{Nb}^{5+}$ ,  $\text{Mo}^{6+}$ ,  $\text{W}^{6+}$ ) adopt the  $\alpha$  and  $\beta$  isomers, which have the greatest number of corner-linked trimers and large distances between metal centers. Rotation from  $\alpha$  to  $\beta$  is favored for more negative clusters; with either reduction of the W/Mo, or a lower-charged central cation.<sup>31</sup> Metals with a lower charge ( $\text{Al}^{3+}$ ,  $\text{Cr}^{3+}$ ,  $\text{Ga}^{3+}$ ) form the  $\delta$  and  $\epsilon$ -isomers (or derivatives thereof) which have the greatest degree of edge-sharing between trimers and smallest distance between metal centers.<sup>7,10,11,14,57</sup> Additionally, the  $\delta$ -Keggin is represented as a building block in  $\text{Fe}^{3+}$ -ferrihydrite.<sup>3</sup> Edge-sharing increases



**Scheme 1** Thermodynamic cycle for  $\beta$ - $\text{NaSn}_{12}$ .

stability by adding rigidity to the molecule; so this is the energetic tradeoff for increased metal–metal repulsion. Presumably the lower-charged cations permit this edge-sharing, since the repulsion is less. All of the clusters in this investigation contain Sn having a +4 oxidation state, which lies between metal charges for experimentally observed Keggin ions, consistent with progression of the favored isomers from  $\alpha$  to  $\epsilon$ .

## Conclusions

To summarize, our one-step, reproducible synthesis of pure and high yield sodium-centered butyltin Keggin ions enables studying thin film deposition and lithographic mechanisms, which is a topic of forthcoming papers. Unlike the related Sn<sub>12</sub>,  $\beta,\gamma$ -NaSn<sub>12</sub> is crystallized readily without counterions, both increasing the simplicity of the synthesis, as well as improving the yield, purity, and reproducibility. The difficulties that arise in reproducibility of synthesis of related Sn<sub>12</sub> was made evident in the study of these Keggin ions. Because the ligands (methoxy and hydroxyl) are extremely labile, crystallizing the clusters with ligands that can also serve as counterions exacerbates the challenge. Although the Sn-butyl bond is hydrolytically inert, the bridging hydroxide ligands of alkyl tin clusters readily exchange in response to solution conditions. Not only are the ligands of the BuSn Keggin ions labile, but also the connectivity between the trimers. Computational results provide essential insights toward helping understand the nature of this unique system that favors lower symmetry Keggin isomers. With this study, we have computationally and experimentally confirmed that the tin Keggin ions represent the only Keggin ion family (thus far) that favors the clusters of lower symmetry; providing a balance between corner-linking to minimize cation–cation repulsion, and edge-linking to maximize stability *via* bond formation.

## Conflicts of interest

There are no conflicts of interest to declare.

## Acknowledgements

This work was funded by the National Science Foundation, Center for Chemical Innovation, grant number CHE-1606982. We also acknowledge the support of the Oregon State University NMR Facility funded in part by the National Institutes of Health, HEI Grant 1S10OD018518, and by the M. J. Murdock Charitable Trust grant #2014162.

## References

- J. F. Keggin, *Proc. R. Soc. London, Ser. A*, 1934, **144**(851), 75–100.
- M. E. Fleet, *Acta Crystallogr., Sect. B: Struct. Crystallogr. Cryst. Chem.*, 1981, **37**(4), 917–920.
- F. M. Michel, L. Ehm, S. M. Antao, P. L. Lee, P. J. Chupas, G. Liu, D. R. Strongin, M. A. A. Schoonen, B. L. Phillips and J. B. Parise, *Science*, 2007, **316**(5832), 1726–1729.
- L. Pauling, *Z. Kristallogr. – Cryst. Mater.*, 2015, **84**(1–6), 442–452.
- A. R. Kampf, J. M. Hughes, B. P. Nash and J. Marty, *Am. Mineral.*, 2017, **102**(2), 461–465.
- L. C. W. Baker and J. S. Figgis, *J. Am. Chem. Soc.*, 1970, **92**(12), 3794–3797.
- G. Johansson, L.-O. Gullman, A. Kjekshus and R. Söderquist, *Acta Chem. Scand.*, 1960, **14**, 771–773.
- W. H. Casey, *Chem. Rev.*, 2006, **106**(1), 1–16.
- W. H. Casey, M. M. Olmstead, C. R. Hazlett, C. Lamar and T. Z. Forbes, *Inorganics*, 2015, **3**(1), 21–26.
- O. A. Gerasko, E. A. Mainicheva, D. Y. Naumov, N. V. Kuratieva, M. N. Sokolov and V. P. Fedin, *Inorg. Chem.*, 2005, **44**(12), 4133–4135.
- M. Fairley, K. W. Corum, A. Johns, D. K. Unruh, M. Basile, J. de Groot, S. E. Mason and T. Z. Forbes, *Chem. Commun.*, 2015, **51**(62), 12467–12469.
- L. Allouche, C. Gérardin, T. Loiseau, G. Férey and F. Taulelle, *Angew. Chem., Int. Ed.*, 2000, **39**(3), 511–514.
- J. Rowsell and L. F. Nazar, *J. Am. Chem. Soc.*, 2000, **122**(15), 3777–3778.
- W. Wang, L. B. Fullmer, N. A. G. Bandeira, S. Goberna-Ferrón, L. N. Zakharov, C. Bo, D. A. Keszler and M. Nyman, *Chem*, 2016, **1**(6), 887–901.
- O. Sadeghi, L. N. Zakharov and M. Nyman, *Science*, 2015, **347**(6228), 1359–1362.
- O. Sadeghi, C. Falaise, P. I. Molina, R. Hufschmid, C. F. Campana, B. C. Noll, N. D. Browning and M. Nyman, *Inorg. Chem.*, 2016, **55**(21), 11078–11088.
- S. Saha, D.-H. Park, D. C. Hutchison, M. R. Olsen, L. N. Zakharov, D. Marsh, S. Goberna-Ferrón, R. T. Frederick, J. T. Diulus, N. Kenane, *et al.*, *Angew. Chem., Int. Ed.*, 2017, **56**(34), 10140–10144.
- H. Reuter, *Angew. Chem., Int. Ed. Engl.*, 1991, **30**(11), 1482–1484.
- V. Baskar, M. Shanmugam, M. Helliwell, S. J. Teat and R. E. P. Winpenny, *J. Am. Chem. Soc.*, 2007, **129**(11), 3042–3043.
- H. Puff and H. Reuter, *J. Organomet. Chem.*, 1989, **373**(2), 173–184.
- C. Eychenne-Baron, F. Ribot and C. Sanchez, *J. Organomet. Chem.*, 1998, **567**(1–2), 137–142.
- C. Eychenne-Baron, F. Ribot, N. Steunou, C. Sanchez, F. Fayon, M. Biesemans, J. C. Martins and R. Willem, *Organometallics*, 2000, **19**(10), 1940–1949.
- B. Cardineau, R. Del Re, M. Marnell, H. Al-Mashat, M. Vockenhuber, Y. Ekinci, C. Sarma, D. A. Freedman and R. L. Brainard, *Microelectron. Eng.*, 2014, **127**, 44–50.
- F. Ribot, C. Eychenne-Baron, F. Fayon, D. Massiot and B. Bresson, *Main Group Met. Chem.*, 2002, **25**(1–2), 115–119.

- 25 A. Márquez, J. Anguiano, G. González and J. Fernández Sanz, *J. Organomet. Chem.*, 1995, **486**(1), 45–50.
- 26 M. R. Stem and M. L. Ellzey, *Struct. Chem.*, 2010, **21**(1), 43–58.
- 27 P. Matczak, *Comput. Theor. Chem.*, 2013, **1013**(Supplement C), 7–14.
- 28 M. R. Adams, E. A. C. Bushnell, T. Bruce Grindley and R. J. Boyd, *Comput. Theor. Chem.*, 2014, **1050**(Supplement C), 7–14.
- 29 S.-H. Wang and S. A. Jansen, *Chem. Mater.*, 1994, **6**(11), 2130–2137.
- 30 I. A. Weinstock, J. J. Cowan, E. M. G. Barbuzzi, H. Zeng and C. L. Hill, *J. Am. Chem. Soc.*, 1999, **121**(19), 4608–4617.
- 31 X. López, J. M. Maestre, C. Bo and J.-M. Poblet, *J. Am. Chem. Soc.*, 2001, **123**(39), 9571–9576.
- 32 K. M. Sundaram, W. A. Neiwert, C. L. Hill and I. A. Weinstock, *Inorg. Chem.*, 2006, **45**(3), 958–960.
- 33 A. Sartorel, M. Carraro, A. Bagno, G. Scorrano and M. Bonchio, *Angew. Chem., Int. Ed.*, 2007, **46**(18), 3255–3258.
- 34 X. López, J. J. Carbó, C. Bo and J. M. Poblet, *Chem. Soc. Rev.*, 2012, **41**(22), 7537–7571.
- 35 K. Sugahara, S. Kuzuya, T. Hirano, K. Kamata and N. Mizuno, *Inorg. Chem.*, 2012, **51**(14), 7932–7939.
- 36 S. E. Smart, J. Vaughn, I. Pappas and L. Pan, *Chem. Commun.*, 2013, **49**(97), 11352–11354.
- 37 C. R. Armstrong, W. H. Casey and A. Navrotsky, *Proc. Natl. Acad. Sci. U. S. A.*, 2011, **108**(36), 14775–14779.
- 38 C. A. Ohlin, J. R. Rustad and W. H. Casey, *Dalton Trans.*, 2014, **43**(39), 14533–14536.
- 39 F.-Q. Zhang, W. Guan, Y.-T. Zhang, M.-T. Xu, J. Li and Z.-M. Su, *Inorg. Chem.*, 2010, **49**(12), 5472–5481.
- 40 J. Ilavsky and P. R. Jemian, *J. Appl. Crystallogr.*, 2009, **42**(2), 347–353.
- 41 X. Zuo, G. Cui, K. M. Merz, L. Zhang, F. D. Lewis and D. M. Tiede, *Proc. Natl. Acad. Sci. U. S. A.*, 2006, **103**(10), 3534–3539.
- 42 H. E. Gottlieb, V. Kotlyar and A. Nudelman, *J. Org. Chem.*, 1997, **62**(21), 7512–7515.
- 43 G. M. Sheldrick, *Siemens Area Detect. Absorpt. Correct. Program*, 1998.
- 44 G. M. Sheldrick, *Acta Crystallogr., Sect. C: Struct. Chem.*, 2015, **71**(1), 3–8.
- 45 M. J. Frisch, *et al.*, *Gaussian 09*, Gaussian, Inc., Wallingford, CT, 2013.
- 46 A. D. Becke, *J. Chem. Phys.*, 1993, **98**(7), 5648–5652.
- 47 P. C. Hariharan and J. A. Pople, *Theor. Chim. Acta*, 1973, **28**(3), 213–222.
- 48 W. R. Wadt and P. J. Hay, *J. Chem. Phys.*, 1985, **82**(1), 284–298.
- 49 A. V. Marenich, C. J. Cramer and D. G. Truhlar, *J. Phys. Chem. B*, 2009, **113**(18), 6378–6396.
- 50 R. Krishnan, J. S. Binkley, R. Seeger and J. A. Pople, *J. Chem. Phys.*, 1980, **72**(1), 650–654.
- 51 D. Dakternieks, H. Zhu, E. R. T. Tiekink and R. Colton, *J. Organomet. Chem.*, 1994, **476**(1), 33–40.
- 52 J. Ho and M. L. Coote, *Theor. Chem. Acc.*, 2010, **125**(1–2), 3.
- 53 J. A. Fernández, X. López and J. M. Poblet, *J. Mol. Catal. A: Chem.*, 2007, **262**(1), 236–242.
- 54 A. Kremleva, P. A. Aparicio, A. Genest and N. Rösch, *Electrochim. Acta*, 2017, **231**, 659–669.
- 55 X. López and J. M. Poblet, *Inorg. Chem.*, 2004, **43**(22), 6863–6865.
- 56 J.-H. Son and W. H. Casey, *Chem. Commun.*, 2015, **51**(8), 1436–1438.
- 57 E. Montargès, L. J. Michot and P. Ildefonse, *Microporous Mesoporous Mater.*, 1999, **28**(1), 83–101.